Madras Journal Series Pvt Ltd
Advanced Materials & Applications
Adv. Mater. App. 5 (2020) 15-23
ISSN: 2582-5070

Influence of titanium oxide nanoparticles on corrosion parameters and properties of tin based solder alloys

Abu Bakr El-Bediwi* and Reham Samir

Physics Department, Faculty of Science, Mansoura University, Egypt.

***Corresponding author:** baker_elbediwi@yahoo.com

Received 25 January 2020, Received in final form 07 February 2020, Accepted 07 February 2020

Abstract

Effect of adding titanium oxide nanoparticles (Ti_2O) on structure, electrochemical corrosion parameters, melting temperature and spreading on copper substrate for $Sn_{60}Bi_{29.3}Sb_6Zn_4Cu_{0.7}$ alloy are studied. Titanium oxide has powerful effect on corrosion parameters and wettability of tin penta alloy. Matrix structure as formed phases and solid solution/ or undetected phases of $Sn_{60}Bi_{29.3}Sb_6Zn_4Cu_{0.7}$ alloy changed after adding titanium oxide. $Sn_{60}Bi_{28.4}Sb_6Zn_4Cu_{0.7}(Ti_2O)_{0.9}$ alloy has high corrosion resistance. Melting temperature of $Sn_{60}Bi_{29.3}Sb_6Zn_4Cu_{0.7}$ alloy varied after adding titanium oxide and $Sn_{60}Bi_{28.1}Sb_6Zn_4Cu_{0.7}(Ti_2O)_{1.2}$ alloy has lowest value. Also titanium oxide improve corrosion parameters and spreading of penta tin based alloy.

Keywords: *Corrosion parameters, lattice strain, titanium oxide, solder properties, tin- bismuth based alloys*

1. Introduction

Tin-lead solder alloys are widely used in electronics because they have convenient material properties and low cost. Due to the inherent toxicity of lead, environmental regulations around the world have been targeted to eliminate the usage of it. This has encouraged the development of lead free solder alloys and enhanced the research activities in this field. Most lead free solder alloys have higher tin content which caused the growth of tin whiskers, higher melting temperature and cost more. Lower tin content in solder alloy increased pasty range, decreased wetting properties and raised the liquidus temperature whilst of course reducing the cost. The contact angle and corrosion rate $Sn_{82}Bi_{15}Zn_3$ alloy decreased after adding different ratio from titanium oxide [1]. Microstructure, melting temperature, spreading, hardness and corrosion parameters of tin based alloys changed after adding titanium oxide [1-5]. Tin- zinc eutectic alloy has been considered as a candidate for lead free solder materials because it has low melting point, excellent mechanical properties and low cost [6- 8]. Some researchers [9-12] worked to improve the properties of Sn-Zn alloy by adding small amount of Bi or Cu or In or Ag or Al or Ga or Sb or Cr or Ni or Ge elements to develop ternary and even quaternary lead free alloys. Also several elements as Zn, Bi, Cu, Ag, Sb and so on added to tin based alloys to improve their solder properties [13-15]. The aim of this work is to study the effect of adding titanium oxide on structure, corrosion parameters, melting temperature and spreading of $Sn_{60}Bi_{29.3}Sb_6Zn_4Cu_{0.7}$ alloy.

2. Materials and methods

2.1. Preparation of samples

High purity metals as tin, bismuth, antimony, zinc, copper and titanium oxide are used to prepare used alloys. These mixed metals with Ti_2O by weight percentage are melted then casted on substrate in air. The used samples are prepared in convenient shape for all tests.

2.2. Characterization

Structure of used alloys is studied using Shimadzu X–ray Diffractometer {(Dx–30, Japan) Cu–Kα radiation with λ=1.54056 Å at 45 kV and 35 mA and Ni–filter, in the angular range 2θ ranging from 0 to 100° in continuous mode with a scan speed 5 deg/min} and scanning electron microscope (JEOL JSM-6510LV, Japan). The polarization studies were performed using Gamry Potentiostat/Galvanostat with a Gamry framework system based on ESA 300. Gamry applications include software DC105 for corrosion measurements and Echem Analyst version 5.5 software packages for data fitting. The differential scanning calorimetry (DSC) thermographs were obtained by Universal V4-5A TA instrument with heating rate 10 k/min in the temperature range 0-400 °C.

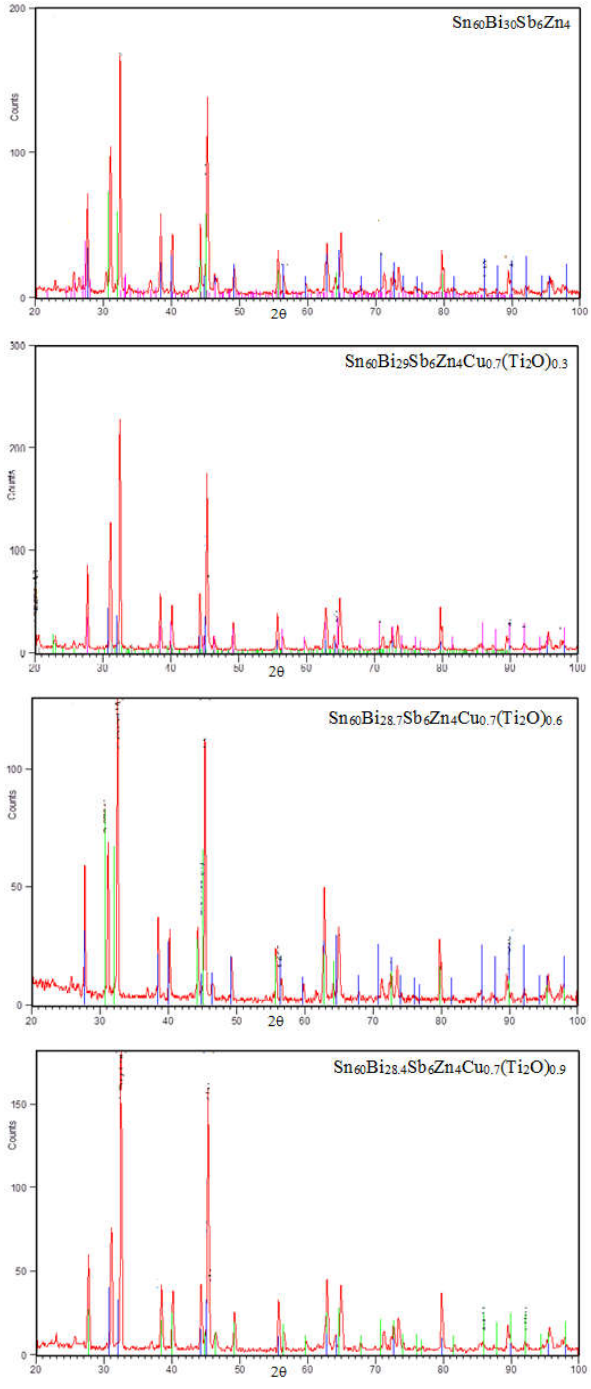

Fig. 1 *X-ray diffraction patterns of* $Sn_{60}Bi_{29.3-x}Sb_6Zn_4Cu_{0.7}(Ti_2O)_x$ *alloys*

3. Results and discussion

3.1. X-ray diffraction studies

Fig. 1 shows x-ray diffraction patterns for $Sn_{60}Bi_{29.3-x}Sb_6Zn_4Cu_{0.7}(Ti_2O)_x$ (x=0, 0.3, 0.6, 0.9 and 1.2) alloys which have sharp lines corresponding to tetragonal β-Sn phase, hexagonal Bi phase, Zn phase, undetected phases/or dissolved atoms formed a solid solution as Ti_2O or Sb or Cu. The details of x-ray analysis, (peak intensity, peak broadness and peak position) from device and cards are listed in Table 1, show that matrix alloy is changed after adding different ratio from titanium oxide. Lattice microstrain (ε) for $Sn_{60}Bi_{29.3}Sb_6Zn_4Cu_{0.7}$ alloy calculated from the relation between full widths half maximum (FWHM) and 4tanθ, Fig. 2, is varied after adding Ti_2O as presented in Table 2.

Table 1 *X-ray diffraction analysis of* $Sn_{60}Bi_{29.3-x}Sb_6Zn_4Cu_{0.7}(Ti_2O)_x$ *alloys*

X-ray analysis of $Sn_{60}Bi_{30}Sb_6Zn_4$ alloy						
2θ	d Å	Int. %	Phase	hkl	FWHM	Area
25.64	3.474	7.33	Bi	101	0.236	2.75
27.63	3.227	41.15	Bi	012	0.216	14.12
31.07	2.878	60.43	Sn	101	0.196	18.86
32.43	2.760	100	Sn	101	0.196	31.21
36.94	2.433	5.15	Zn	002	0.393	3.22
38.40	2.344	33.04	Bi	104	0.275	14.44
40.16	2.245	24.35	Bi	110	0.275	10.64
44.26	2.046	29.1	Bi	015	0.216	9.99
45.30	2.001	83.46	Sn	211	0.216	28.65
46.51	1.952	6.19	Bi	113	0.472	4.63
49.18	1.852	12.25	Bi	202	0.275	5.35
55.65	1.651	18.76	Sn	301	0.236	7.03
56.52	1.628	6.53	Bi	024	0.314	3.26
62.84	1.478	21.5	Sn	112	0.236	8.05
64.89	1.436	24.91	Sn	112	0.236	9.33
71.28	1.322	7.1	Bi	009	0.314	3.55
73.38	1.290	10.15	Sn	411	0.236	3.8
79.71	1.202	18.71	Sn	312	0.177	5.25
85.88	1.131	2.58	Bi	20	0.944	3.86
89.64	1.093	6.8	Bi	306	0.472	5.09
95.76	1.038	3.93	Sn	332	0.768	6.47

X-ray analysis of $Sn_{60}Bi_{29}Sb_6Zn_4Cu_{0.7}(Ti_2O)_{0.3}$ alloy						
2θ	d Å	Int. %	Phase	hkl	FWHM	Area
20.38	4.356	4.97	SbCu	001	0.472	5.14
22.92	3.879	3.84	Bi	003	0.472	3.97
27.73	3.216	36.57	Bi	012	0.255	20.51
31.12	2.873	54.67	Sn	101	0.216	25.94
32.50	2.754	100	Sn	101	0.255	56.08
38.46	2.340	24.33	Bi	104	0.275	14.69
40.17	2.244	19.53	Bi	110	0.216	9.27
44.22	2.047	20.98	Bi	015	0.295	13.58
45.31	2.001	76.37	Sn	211	0.216	36.24
46.36	1.958	6.2	Bi	113	0.314	4.28
49.31	1.847	9.28	Bi	202	0.177	3.6
55.67	1.650	15.28	Sn	301	0.255	8.57
56.52	1.628	4.91	Bi	024	0.236	2.54
59.75	1.547	3.55	Bi	107	0.314	2.45
62.87	1.478	18.33	Sn	112	0.354	14.24
64.11	1.452	5.43	Sn	400	0.236	2.81
64.90	1.436	22.57	Sn	321	0.177	8.76
71.29	1.322	5.08	Bi	009	0.314	3.5
72.69	1.300	6.82	Bi	300	0.314	4.71
73.41	1.289	10.08	Sn	411	0.196	4.35
79.73	1.202	18.98	Sn	312	0.157	6.55
89.67	1.093	4.47	Bi	306	0.472	4.63
92.13	1.070	2.65	Bi	321	0.472	2.74
95.77	1.039	5.21	Sn	332	0.472	5.4
97.75	1.022	2.3	Bi	134	0.768	5.24

X-ray analysis of $Sn_{60}Bi_{28.7}Sb_6Zn_4Cu_{0.7}(Ti_2O)_{0.6}$ alloy						
2θ	d Å	Int. %	Phase	hkl	FWHM	Area
27.72	3.217	42.77	Bi	012	0.196	10.5
31.16	2.870	50.43	Sn	101	0.196	12.38
32.54	2.751	100	Sn	101	0.216	27.01
38.52	2.336	26.65	Bi	104	0.216	7.2
40.2	2.243	22.9	Bi	110	0.177	5.06
44.31	2.044	23.61	Bi	202	0.216	6.38
45.37	1.998	86.98	Bi	202	0.196	21.36
46.43	1.955	5.53	Bi	113	0.393	2.71
49.18	1.852	10.88	Bi	202	0.196	2.67
55.69	1.650	14.17	Sn	301	0.216	3.83
56.60	1.625	6.49	Bi	024	0.236	1.91
59.81	1.546	4.01	Bi	107	0.472	2.37
62.86	1.478	36.33	Sn	112	0.216	9.81
64.91	1.436	22.71	Sn	112	0.314	8.92
72.75	1.299	7.61	Sn	420	0.551	5.23
73.52	1.288	11.09	Sn	411	0.314	4.36
79.76	1.202	20.94	Sn	312	0.157	4.11
89.69	1.093	5.52	Bi	306	0.472	3.25
95.69	1.039	5.79	Sn	332	0.768	7.5

X-ray analysis of $Sn_{60}Bi_{28.4}Sb_6Zn_4Cu_{0.7}(Ti_2O)_{0.9}$ alloy						
2θ	d Å	Int. %	Phase	hkl	FWHM	Area
27.69	3.220	32.21	Bi	012	0.334	18.68
31.06	2.879	40.4	Sn	101	0.295	20.68
32.46	2.757	100	Sn	101	0.275	47.77
37.02	2.428	2.32	Bi	104	0.433	1.74
38.43	2.341	21.52	Bi	104	0.295	11.02
40.13	2.246	19.31	Bi	110	0.314	10.54
44.28	2.045	21.58	Bi	015	0.255	9.57
45.30	2.001	87.04	Sn	211	0.295	44.55
46.37	1.958	4.99	Bi	113	0.393	3.4
49.20	1.851	13.02	Bi	202	0.275	6.22
55.68	1.650	17.01	Sn	301	0.295	8.7
56.51	1.628	6.32	Bi	024	0.314	3.45
62.87	1.478	23.3	Sn	112	0.255	10.34
64.86	1.437	20.08	Sn	112	0.236	8.22
71.23	1.323	5.63	Bi	009	0.314	3.07
73.36	1.290	10.01	Sn	411	0.196	3.42
79.70	1.203	17.77	Sn	312	0.216	6.67
85.64	1.134	2.02	Bi	119	0.944	3.31
89.55	1.094	8.12	Bi	306	0.314	4.43
95.80	1.038	5.48	Sn	332	0.576	7.39

X-ray analysis of $Sn_{60}Bi_{28.1}Sb_6Zn_4Cu_{0.7}(Ti_2O)_{1.2}$ alloy						
2θ	d Å	Int. %	Phase	hkl	FWHM	Area
27.67	3.223	30.5	Bi	012	0.196	7.42
31.06	2.879	48.52	Sn	101	0.216	12.98
32.51	2.753	100	Sn	101	0.236	29.17
38.47	2.340	22.1	Bi	104	0.216	5.91
40.14	2.246	19.28	Bi	110	0.196	4.69
44.31	2.044	27.37	Bi	015	0.236	7.98
45.33	2.000	76.92	Sn	211	0.255	24.31
49.26	1.849	12.76	Bi	202	0.314	4.96
55.74	1.649	19.23	Sn	301	0.196	4.67
56.56	1.627	6.43	Bi	024	0.314	2.5
62.89	1.477	27.12	Sn	112	0.314	10.55
64.92	1.436	24.27	Sn	321	0.275	8.26
71.33	1.322	6.02	Bi	009	0.472	3.51
72.70	1.300	10.56	Sn	420	0.236	3.08
73.49	1.288	8.64	Sn	411	0.314	3.36
79.72	1.202	23.6	Sn	312	0.118	3.44
85.31	1.137	3.12	Bi	119	0.944	3.64
89.70	1.093	5.27	Bi	306	0.472	3.07
92.21	1.069	3.12	Bi	321	0.472	1.82
95.85	1.037	5.09	Sn	332	0.768	6.53

Table 2 *lattice microstrain of* $Sn_{60}Bi_{29.3-x}Sb_6Zn_4Cu_{0.7}(Ti_2O)_x$

Alloys	ε
$Sn_{60}Bi_{30}Sb_6Zn_4$	0.117
$Sn_{60}Bi_{29}Sb_6Zn_4Cu_{0.7}(Ti_2O)_{0.3}$	0.055
$Sn_{60}Bi_{28.7}Sb_6Zn_4Cu_{0.7}(Ti_2O)_{0.6}$	0.118
$Sn_{60}Bi_{28.4}Sb_6Zn_4Cu_{0.7}(Ti_2O)_{0.9}$	0.101
$Sn_{60}Bi_{28.1}Sb_6Zn_4Cu_{0.7}(Ti_2O)_{1.2}$	0.129

3.2. Scanning electron micrographs analysis

Scanning electron micrographs (SEM) for $Sn_{60}Bi_{29.3-x}Sb_6Zn_4Cu_{0.7}(Ti_2O)_x$ (x= 0, 0.3, 0.6, 0.9 and 1.2) alloys are shown in Fig. 3. SEM of $Sn_{60}Bi_{30}Sb_6Zn_4$ alloy has dendrite structure contained different geometric shape as a tin phase (gray color), bismuth phase (black color) and spherical small grains white/or gray as antimony or zinc or intermetallic compounds formed in matrix alloy. $Sn_{60}Bi_{29}Sb_6Zn_4Cu_{0.7}(Ti_2O)_{0.3}$ alloy has a homogenous structure from tin phase (gray color) contained slabs with different size (black color) as bismuth phase and spherical grains white/or gray presented undetected or detected phases (Sb or Zn or Ti_2O or intermetallic compounds). $Sn_{60}Bi_{28.7}Sb_6Zn_4Cu_{0.7}(Ti_2O)_{0.6}$ alloy has a heterogeneous structure tin phase as a gray color contained bismuth phase (rods with different size and orientation) as black color and spherical shape and slabs in matrix or around grains (gray or white color) as Sb or Cu or Zn or Ti_2O or intermetallic compounds. $Sn_{60}Bi_{28.4}Sb_6Zn_4Cu_{0.7}(Ti_2O)_{0.9}$ alloy has a homogenous matrix structure tin phase as a gray color contained bismuth phase as black color, spherical and slabs (Sb or Cu or Zn or Ti_2O or intermetallic compounds) as gray color. $Sn_{60}Bi_{28.1}Sb_6Zn_4Cu_{0.7}(Ti_2O)_{1.2}$ alloy has a lamellar structure from tin phase (gray color) and bismuth phase (black color) contained spherical and slabs around lamellar and inside (gray and white color). From SEM analysis it's obvious that, adding titanium oxide changed matrix structure of $Sn_{60}Bi_{29.3}Sb_6Zn_4Cu_{0.7}$ alloy.

3.3 Solder properties

Fig. 4 shows the differential scanning calorimetric (DSC) graphs of $Sn_{60}Bi_{29.3-x}Sb_6Zn_4Cu_{0.7}(Ti_2O)_x$ (x=0, 0.3, 0.6, 0.9 and 1.2) alloys. DSC graphs (shape, broadness and intensity) of $Sn_{60}Bi_{30}Sb_6Zn_4$ alloy changed after adding Ti_2O. Melting temperature of $Sn_{60}Bi_{29.3}Sb_6Zn_4Cu_{0.7}$ alloy is varied after adding Ti_2O as listed in Table 3 and it is less than based eutectic alloys (Sn-Sb or Sn- Cu) and less than or very closed with a commercial lead- tin solder. The spreading of molten $Sn_{60}Bi_{29.3-x}Sb_6Zn_4Cu_{0.7}(Ti_2O)_x$ (x=0, 0.3, 0.6, 0.9 and 1.2) alloys on copper substrate in air is different as shown in Fig. 5 because it's dependent in alloy composition.

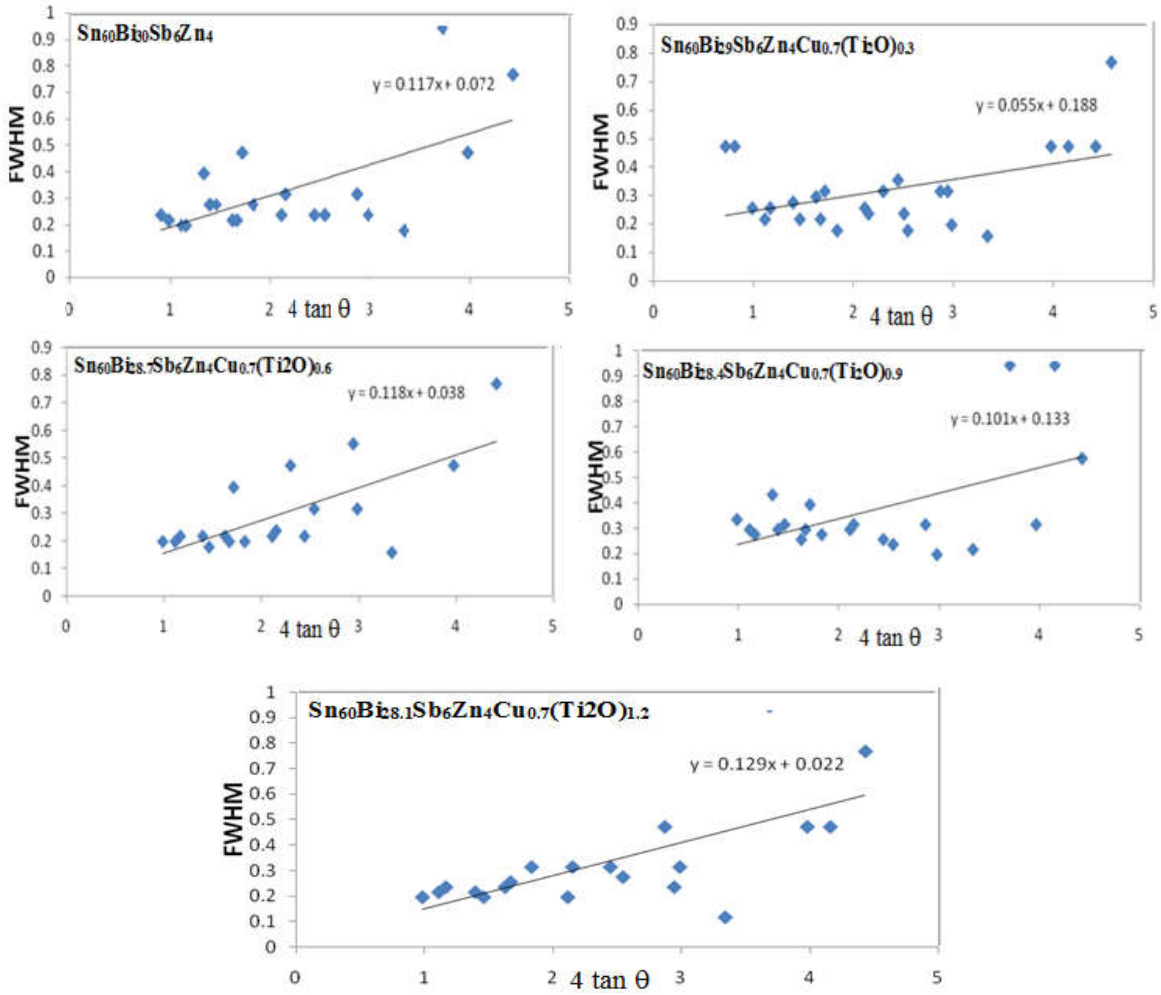

Fig. 2 *FWHM versus 4tanθ for* $Sn_{60}Bi_{29.3-x}Sb_6Zn_4Cu_{0.7}(Ti_2O)_x$ *alloys*

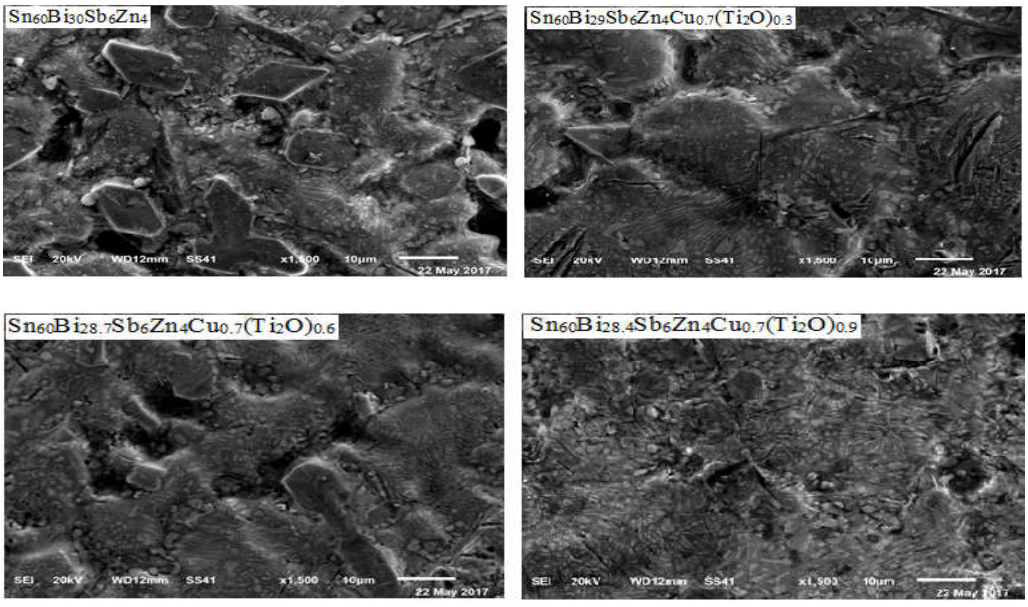

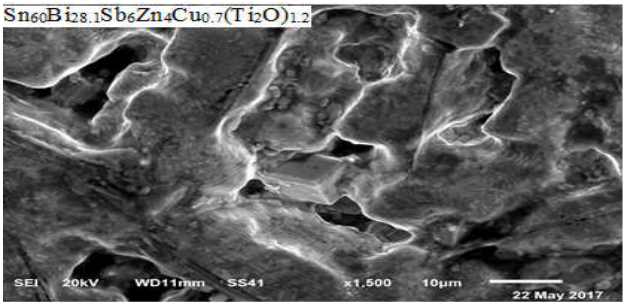

Fig. 3 *SEM of $Sn_{60}Bi_{29.3-x}Sb_6Zn_4Cu_{0.7}(Ti_2O)_x$ alloys*

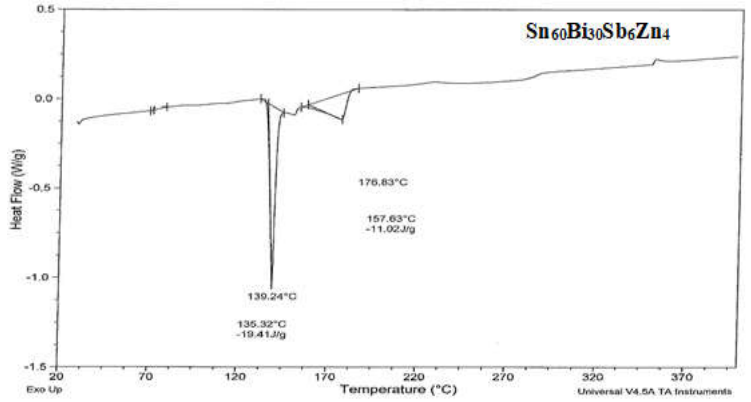

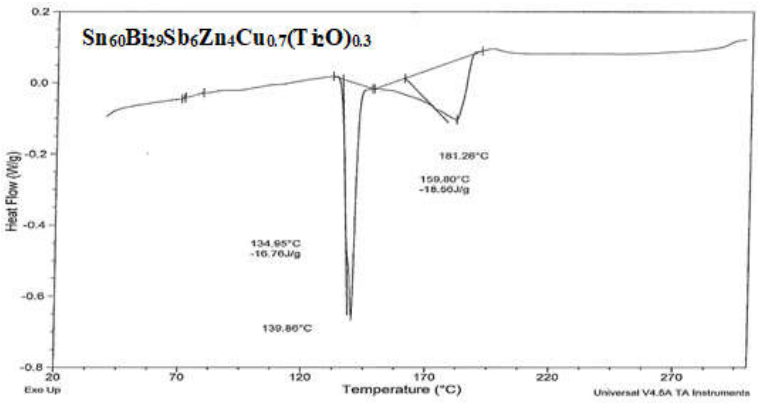

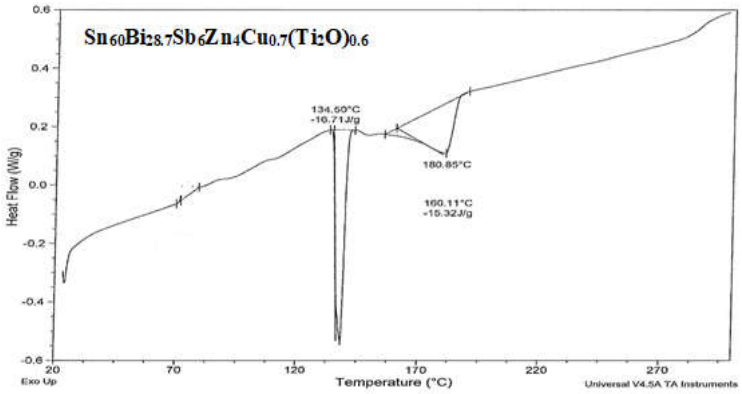

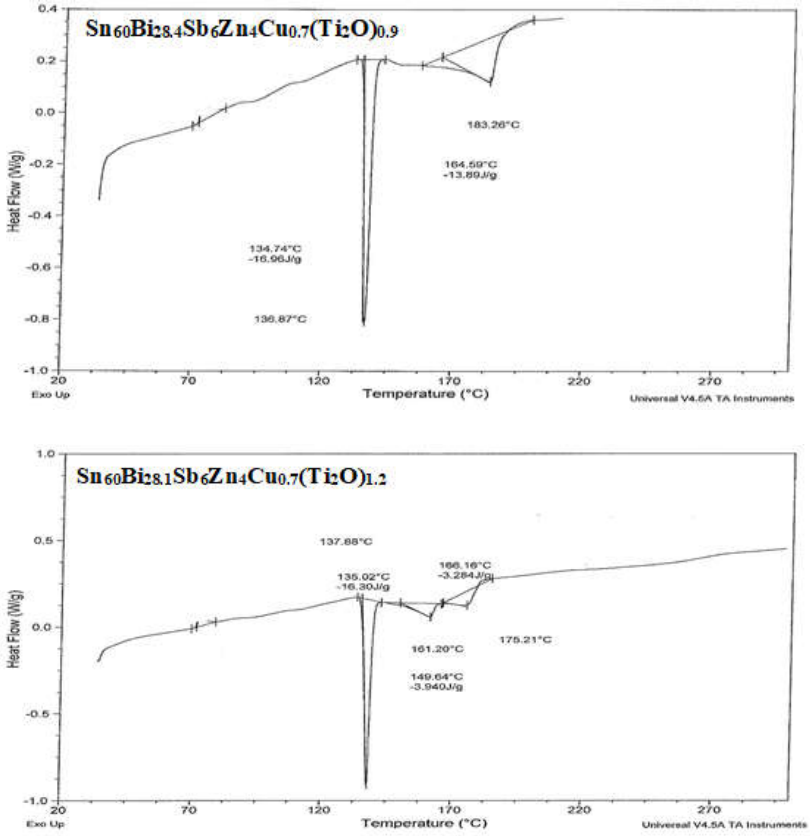

Fig. 4 *DSC of $Sn_{60}Bi_{29.3-x}Sb_6Zn_4Cu_{0.7}(Ti_2O)_x$ alloys*

Fig. 5 *Spreading of used alloys on copper substrate in air*

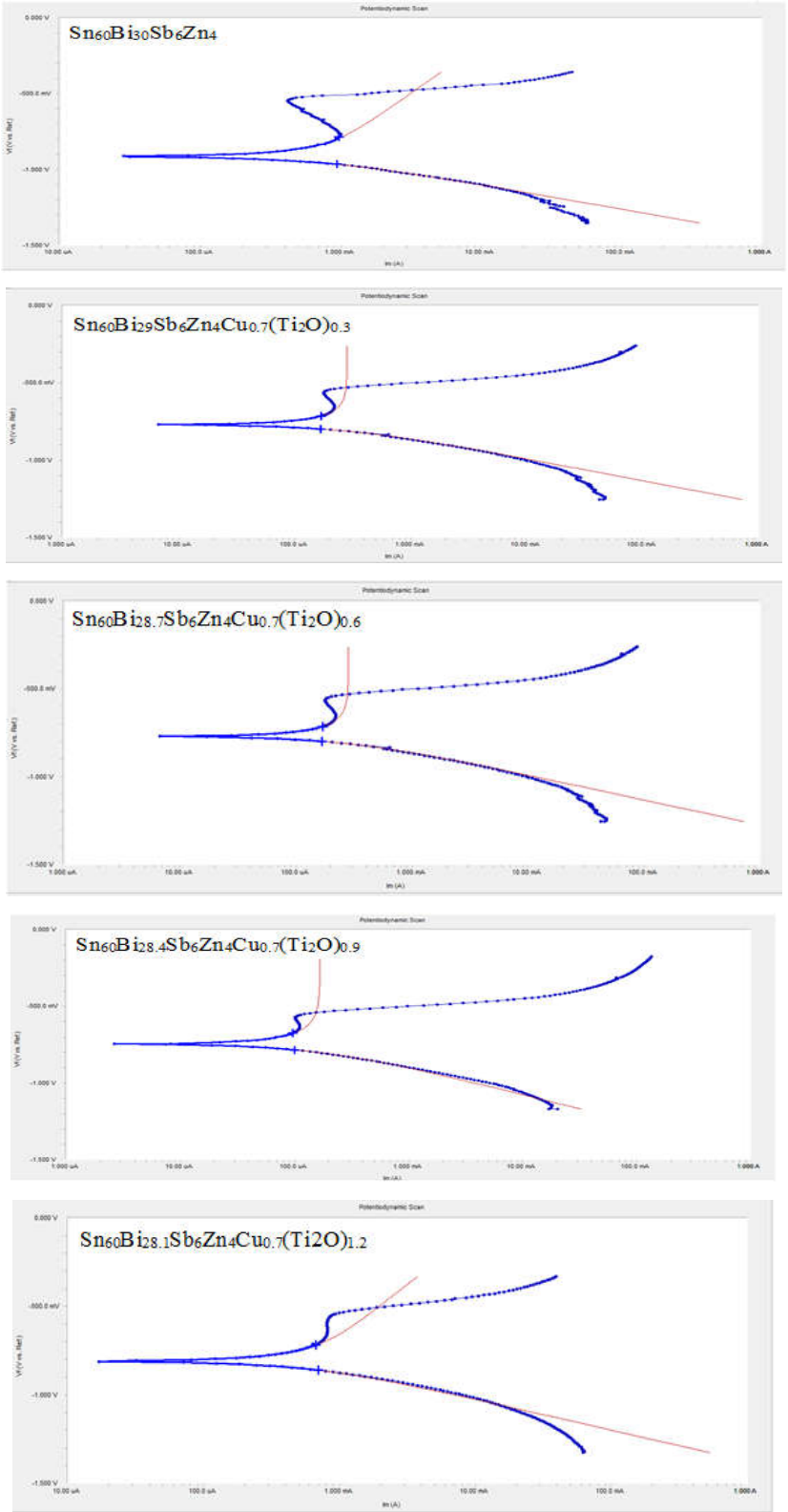

Fig. 6 *Electrochemical polarization curves of* $Sn_{60}Bi_{29.3-x}Sb_6Zn_4Cu_{0.7}(Ti_2O)_x$ *alloys*

Table 3 *Melting temperature of* $Sn_{60}Bi_{29.3-x}Sb_6Zn_4Cu_{0.7}(Ti_2O)_x$ *alloys*

Alloys	Melting temperature °C
$Sn_{96}Zn_4$	216.4
$Sn_{95}Sb_5$	223
$Sn_{60}Bi_{30}Sb_6Zn_4$	176.83
$Sn_{60}Bi_{29}Sb_6Zn_4Cu_{0.7}(Ti_2O)_{0.3}$	187.3
$Sn_{60}Bi_{28.7}Sb_6Zn_4Cu_{0.7}(Ti_2O)_{0.6}$	180.85
$Sn_{60}Bi_{28.4}Sb_6Zn_4Cu_{0.7}(Ti_2O)_{0.9}$	183.26
$Sn_{60}Bi_{28.1}Sb_6Zn_4Cu_{0.7}(Ti_2O)_{1.2}$	175.21

3.4. Corrosion behavior

Fig. 6 shows the electrochemical polarization curves of $Sn_{60}Bi_{29.3-x}Sb_6Zn_4Cu_{0.7}(Ti_2O)_x$ (x=0, 0.3, 0.6, 0.9 and 1.2) alloys in 0.25 M HCl. The corrosion potential of $Sn_{60}Bi_{29.3-x}Sb_6Zn_4Cu_{0.7}(Ti_2O)_x$ alloys exhibited a negative potential. Also the cathodic and the anodic polarization curves showed similar corrosion trends. The corrosion potential (E_{Corr}), corrosion current (I_{Corr}) and corrosion rate ($Corr_{Rate}$) of $Sn_{60}Bi_{29.3-x}Sb_6Zn_4Cu_{0.7}(Ti_2O)_x$ alloys are listed in Table 4. Adding different ratio from $(Ti_2O)_x$ decreased corrosion rate and corrosion current values of $Sn_{60}Bi_{29.3}Sb_6Zn_4Cu_{0.7}$ alloy. $Sn_{60}Bi_{28.4}Sb_6Zn_4Cu_{0.7}(Ti_2O)_{0.9}$ alloy has better corrosion resistance.

Table 4 *Corrosion parameters of* $Sn_{60}Bi_{29.3-x}Sb_6Zn_4Cu_{0.7}(Ti_2O)_x$ *alloys*

Alloys	E_{corr} mV	I_{corr} uA	$Corr_{Rate}$ mpy
$Sn_{60}Bi_{30}Sb_6Zn_4$	-913	719	328.5
$Sn_{60}Bi_{29}Sb_6Zn_4Cu_{0.7}(Ti_2O)_{0.3}$	-771	190	186.83
$Sn_{60}Bi_{28.7}Sb_6Zn_4Cu_{0.7}(Ti2O)_{0.6}$	-770	283	229.3
$Sn_{60}Bi_{28.4}Sb_6Zn_4Cu_{0.7}(Ti_2O)_{0.9}$	-746	186	176.77
$Sn_{60}Bi_{28.1}Sb_6Zn_4Cu_{0.7}(Ti_2O)_{1.2}$	-809	604	276

4. Conclusion

Adding titanium oxide changed matrix structure of $Sn_{60}Bi_{29.3}Sb_6Zn_4Cu_{0.7}$ alloy caused a variation in all measured properties. Corrosion parameters and solder properties of $Sn_{60}Bi_{29.3}Sb_6Zn_4Cu_{0.7}$ alloy are improved after adding titanium oxide.

References:

[1]. A. B. El-Bediwi, R. Samir, "Influence of titanium oxide on structure, corrosion and soldering properties of $sn_{82}bi_{15}zn_3$ alloy", Res. Dev. Material Sci. 6 (2018) 1.

[2]. A. B. El-Bediwi, N. A. El-Shishtawi, M. M. Abdullah, "Influence of titanium dioxide nanoparticles on microstructure, electrochemical corrosion behavior, mechanical and thermal properties of Sn-Al-Bi based alloy", Int. J. Appl. Sci. Biotechnol. 4 (2016) 417.

[3]. A. B El-Bediwi, S. Bader and F. Khalifa, "Study the effect of titanium dioxide on microstructure, electrochemical corrosion parameters, thermal behavior and internal friction of hexa tin-bismuth based alloy", Mat. Sci. Ind. J. 14 (2016) 1.

[4]. A. B. El-Bediwi, M. Grayb, M. Kamal, "Influence of titanium oxide on creep behavior, microstructure and physical properties of tin-antimony and tin-aluminum-antimony based bearing alloys", Inter. J. Sci. Eng. Appl. 4 (2015) 64.

[5]. A. B. El- Bediwi, A. Al- Bawee, M. Kamal, Effect of Titanium Oxide on Structure, Bearing Properties of Tin-Antimony-Lead and Tin-Aluminum Alloys**",** Inter. J. Sci. Eng. Appl. 4 (2015) 46.

[6]. W. Yang, R. W. Messler Jr, Microstructure evolution of eutectic Sn-Ag solder joints", J. Electron. Mater. 23 (1994) 765.

[7]. H. Mavoori, J. Chin, S. Vaynman, et al., "Creep, stress relaxation, and plastic deformation in Sn-Ag and Sn-Zn eutectic solders", J. Electron. Mater. 41 (1997) 1269.

[8]. M. McCormack, S. Jin and G.W. Kammlott, Proceedings of the 1995 IEEE International Symposium on Electronics and the Environment, ISEE, Orlando, FL, USA May 1–3 (1995) 171.

[9]. K. S. Kim, J. M. Yang, C. H. Yu, I. O. Jung, H. H. Kim, "Analysis on interfacial reactions between Snñ Zn solders and theAu/Ni electrolytic-platedAl pad", J. Alloy. Compd. 379 (2004) 314.

[10]. I. E. Anderson, J. C. Foley, B. A. Cook, J. Harringa, R. L. Terpstra, O. Unal, "Alloying effects in near-eutectic Sn-Ag-Cu solder alloys for improved microstructural stability", J. Electron. Mater. 30 (2001) 1050.

[11]. M. McCormack, S. Jin, G. W. Kammlott, H. S. Chen, "New Pb-free solder alloy with superior mechanical properties", Appl. Phys. Lett. 63 (1993) 15.

[12]. A.Z. Miric, A. Grusd, "Lead free alloys", Surf. Mount Technol. 10 (1998) 19.

[13]. M. Abtew, G. Selvaduray, "Lead-free Solders in Microelectronics", Mater. Sci. Eng. Rep. 27 (2000) 95.

[14]. J. H. Vincent, G. Humpston, "Lead-Free Solders for Electronic Assembly", GEC J. Res. 11 (1994) 76

[15]. M. R. Harrison, J. H. Vincent, H. A. H. Steen, "Lead-free reflow soldering for electronics assembly", Sold. Surf. Mount Technol. 13 (2001) 21

